POWER AND ENERGY FUTURE

Open Access
Research Article

Ambient Humidification-Driven Real-Time Passive Solar Cell Cooling via Hygroscopic Hydrogel

Yuan Chang, Wei Yan, Haoran Li, Wenpeng Hong, and Yurong He

***Abstract*—Evaporative cooling of hygroscopic hydrogels has emerged as a cost-effective and environmentally benign approach for the thermal management of solar cells. However, the cooling capacity of hygroscopic media is largely irreversible under daylight illumination, posing a critical bottleneck to sustaining all-day passive cooling. This work proposes a real-time passive cooling (RTPC) strategy driven by ambient humidification, which enables continuous water harvesting and cyclic evaporation via a hygroscopic hydrogel. Specifically, the heat emitted by the solar cell is harnessed to drive spontaneous evaporation of moisture within a closed water tank, thereby constructing a persistent high-humidity environment. This integrated high-humidity RTPC system, coupled with the elevated operating temperature of the solar cell, facilitates the continuous adsorption–desorption cycle of water molecules by the hydrogel, ultimately realizing sustained evaporative cooling for the solar cell. The hygroscopic hydrogel exhibits a water uptake capacity of 1.7 $g \cdot g^{-1}$ at 25 °C and 90% relative humidity (RH). More importantly, under 1.0 sun irradiation, the proposed device reduces the average temperature of the solar cell surface and backsheet by ~ 10 and ~ 15 °C, respectively, leading to an enhancement of 6.0% in open-circuit voltage. This work demonstrates an effective approach for sustainable water replenishment of the hygroscopic hydrogel, thereby enabling all-day passive cooling of solar cells.**

***Index Terms*—Passive solar cell cooling, real-time regeneration, hygroscopic hydrogel, sustainable water collection, environmental humidification.**

ABBREVIATION

AM	acrylamide
AWH	atmospheric water harvesting
CCD	charge-coupled device
KPS	potassium persulfate
MBAA	N,N-methylenedi acrylamide
PCM	phase change materials
PV	photovoltaic
RH	relative humidity
RTPC	real-time passive cooling
TEMED	N,N,N',N'-tetramethylethylenediamine

Manuscript received 20 November, 2025; accepted 25 January, 2026. *(Corresponding authors: Haoran Li, e-mail: haoran@neepu.edu.cn and Yurong He, e-mail: rong@hit.edu.cn)*

Y. Chang, W. Yan, H. Li and W. Hong are with the National & Local Joint Engineering Laboratory for Multi-Energy Complementary and High-Efficiency Energy Supply Management Technology, School of Energy and Power Engineering, Northeast Electric Power University, Jilin, 132012, China.

Y. He is with the Heilongjiang Key Laboratory of New Energy Storage Materials and Processes, School of Energy Science and Engineering, Harbin Institute of Technology, Harbin 150001, China.

Color versions of one or more of the figures in this paper are available online at https://doi.org/10.26599/PEF.2026.9650007.

Digital Object Identifier 10.26599/PEF.2026.9650007

I. INTRODUCTION

Sustained advancements in PV technology and annual cost reductions have established PV as an efficient and economically viable clean energy solution on a global scale [1], [2]. However, due to the inherent bandgap limitations of the semiconductor, only a small fraction of photons are converted into electricity. The remaining photons are converted into waste heat, which not only raises the operating temperature of PV cells but also degrades their power generation efficiency [3], [4], [5]. This issue has spurred the development of various cooling strategies [6], [7], [8], which can be categorized into active and passive cooling [9], [10], [11], [12]. The active cooling device primarily uses mechanical devices like pumps or fans to drive the cooling medium [13], [14], [15], facilitating convective heat transfer between the refrigerant and the high-temperature solar cell. These effectively enhance the operation efficiency of solar cells [16]. Notably, active cooling technologies have advanced from single-sided backplate water spraying to double-sided backplate-panel water spraying [17]. This progress has doubled the power generation efficiency, but it has also been accompanied by a twofold increase in water consumption [18], [19]. Moreover, the substantial amount of water consumed is difficult to recycle [20].

In contrast, passive cooling systems eschew the use of mechanical devices, instead relying on natural convection, radiative cooling, or phase change heat transfer to regulate the temperature of PV modules [21], [22]. For instance, Hudișteanu et al. [23] enhanced the power generation efficiency of PV panels by adopting heat sinks with perforated fins, leveraging natural convection. However, this method is strongly dependent on environmental conditions and exhibits limited effectiveness in windless environments or at low wind speeds. The application of high-emissivity coatings to com-

© The author(s) 2026. Published by Tsinghua University Press.
This is an open access article under the Creative Commons Attribution 4.0 International License (http://creativecommons.org/licenses/by/4.0/).

mercially encapsulated PV panels can promote radiative cooling between the panels and the cold outer space, but it has a low theoretical limit in temperature reduction [24]. PCMs featuring high latent heat and low melting points can reduce the operating temperature of PV panels by more than 8 °C through absorbing waste heat from the panel surface during the melting process [25], [26]. Nevertheless, PCMs typically exhibit low thermal conductivity and low density, which significantly constrains the further enhancement of passive cooling efficiency [27], [28]. Generally, although passive cooling technologies are acclaimed for their structural simplicity and minimal energy consumption, they generally suffer from relatively low cooling performance [29], [30].

Adsorption-based humidity regulation and evaporative cooling are emerging as promising technologies for PV cell cooling. For instance, Li et al. [31] fabricated one-dimensional hygroscopic nanofibers and two-dimensional fabrics via the cross-linking of two hygroscopic polymers, realizing an adsorption capacity of 1.2 $g \cdot g^{-1}$ within 4 h at RH = 90%. Notably, 80% of the absorbed moisture can be desorbed within 10 min under mild heating [32], [33]. Hydrogels, as emerging water harvesters, have attracted significant attention in AWH-assisted passive thermal management [34], [35]. It has been shown that hydrogels can effectively absorb and conduct heat generated by solar cells [36]. The water molecules within the hydrogels can utilize their high latent heat of vaporization (~ 2450 $J \cdot g^{-1}$) during the gas–liquid phase change to achieve significant temperature reduction [37]. Based on this, Pu et al. [38] enhanced the operating efficiency of solar cells by leveraging the evaporative cooling effect of a lithium- and bromine-rich hygroscopic medium. This process relies on the rapid evaporation of moisture to dissipate the waste heat generated by carrier transport within the p–n junction. It reduces the operating temperature of commercial polycrystalline silicon solar cells by 17 °C under 1.0 sun, thereby increasing PV efficiency from 14.5% to 15.5%. However, the performance of the water absorption medium is overly dependent on high ambient humidity during prolonged cooling processes, resulting in poor regeneration capacity of the hydrogel [39]. Therefore, the reabsorption of moisture from the environment by the hydrogel during evaporation is a crucial issue that needs further investigation [40].

This work proposes an RTPC scheme for solar cells, which integrates environmental humidification and hydrogel-based continuous water harvesting. This approach enables the synchronization of water adsorption and desorption, thereby realizing sustainable cooling of solar cells. Specifically, the design leverages the waste heat generated by the solar cells to drive the evaporation of underlying moisture, constructing a high-humidity environment conducive to hydrogel adsorption. Meanwhile, the heat from the backplate drives desorption to cool solar cells. The water within the RTPC device reaches a dynamic equilibrium state: During nighttime, the adsorption capacity of the hydrogel surpasses its desorption capacity, allowing continuous moisture absorption in the high-humidity microenvironment provided by the RTPC system; such a cycle is reset during daytime operation, initiating a new round of RTPC for solar cells. The RTPC system reduces the average temperature of the solar cells by approximately 10 °C and increases the average open-circuit voltage by 6.0% under 1.0 sun illumination. This method avoids the cooling failure problem caused by insufficient water storage in the hydrogel during evaporative cooling, ensuring sustainable water storage.

II. Materials and Methods

A. Chemicals and Materials

LiCl (99%, Aladdin), carbon nanoparticles (CNs, 99.5%, Aladdin), AM (99.9%, Aladdin), MBAA (99%, Aladdin), TEMED (99%, Aladdin), KPS (99.99%, Aladdin), purified water (C'esbon), and solar cells (80 mm × 80 mm, Ningbo Aike Electronic Technology Co., Ltd.). All chemicals were used as received.

B. Preparation of the Hydrogel

The absorbent hydrogel was prepared using the same manner as reported by Li et al. [41]. As shown in Fig. 1, 0.1 g of CNs was added to 10 mL of pure water and processed in an ultrasonic cleaner (PS-100A, Jiekang) for 5 min. Subsequently, 2 g of AM monomer was thoroughly mixed in, followed by the addition of 10 mg of KPS and 0.6 mg of MBAA. Finally, 25 µL of TEMED was introduced as an accelerator to facilitate the polymerization process. The well-mixed solution was then transferred into a petri dish with a diameter of 65 mm and left to stand for 12 h, yielding an AM-CNs hydrogel with

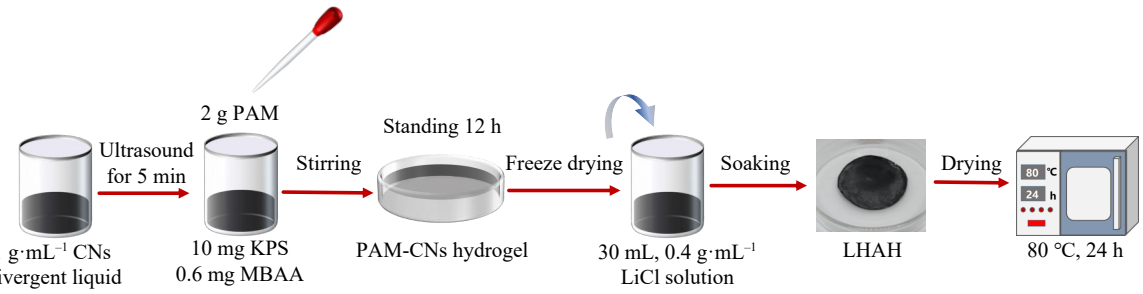

Fig. 1. Preparation process of the LHAH.

a thickness of 4 mm. The precursor amounts were increased proportionally to prepare hydrogels with thicknesses of 6, 8, 10, and 12 mm. The AM-CNs hydrogel matrix was subsequently freeze-dried for 8 h. Thereafter, the freeze-dried AM-CNs hydrogel matrix was soaked in 30 mL of LiCl solution (0.4 g·mL^{-1}) for 48 h to obtain moist salt-based hydrogels. Finally, the hydrogels were dried in an oven (DZF, Lichen) at 80 °C for 12 h to yield a lithium-rich and highly absorbent hydrogel (referring to LHAH).

C. Cooling Experiments

The experimental setup for the RTPC system was constructed as depicted in Fig. 2. A solar simulator (CEL-HXF300-T3, Au-light) was utilized as the input light source, with the irradiance intensity calibrated to 1 sun (1000 W·m^{-2}) via a reference solar cell (CEL-RCCN, Au-light). The open-circuit voltage of the solar cell was recorded at a sampling interval of 1 s using an electrochemical workstation (PGSTA T302N, Autolab). Surface and backplate temperatures of the solar cell were monitored by an infrared thermal imager (T250, FLIR) and a T-type thermocouple connected to a data acquisition unit (34972A, Agilent), respectively. The ambient temperature and relative humidity of the RTPC system were measured using a digital thermometer and hygrometer (TH20BL, MIAOXIN). All procedures were conducted at a room temperature of 26 ± 0.5 °C and RH = 15% ± 5%. The mass variation during the LHAH absorption process was tracked using a high-precision electronic balance (Practicum 313-1CN, Sartorius). The mass change ratio of the hydrogel and its water retention capacity under defined environmental settings were determined through Eqs. (1) and (2), respectively.

$$w_i = \frac{m_i - m_0}{m_0} \tag{1}$$

where w_i represents the mass change rate, with m_i and m_0 denoting the mass of LHAH at time i and the initial mass, respectively.

$$w = m_1 - m_0 \tag{2}$$

where w signifies the amount of water retained by LHAH upon completion of the adsorption process, with m_1 being the mass of LHAH after adsorption and m_0 being its initial mass.

III. Results and Discussion

A. Design Concept of the RTPC Module

Fig. 3(a) illustrates the design scheme of the solar cell cooling structure equipped with an RTPC module. The system consists of a solar cell, a hygroscopic hydrogel, a condensation chamber (180 mm × 90 mm × 80 mm), and a water collection tank (200 mm × 110 mm × 55 mm). The hygroscopic hydrogel is adhered to the back of the solar cell, with a water collection tank located beneath the condensation chamber. The condensation chamber collects the evaporated moisture from the hydrogel for recycling. The condensation chamber and the water tank are interconnected via room-temperature water. The water tank not only serves as a cold source to promote the

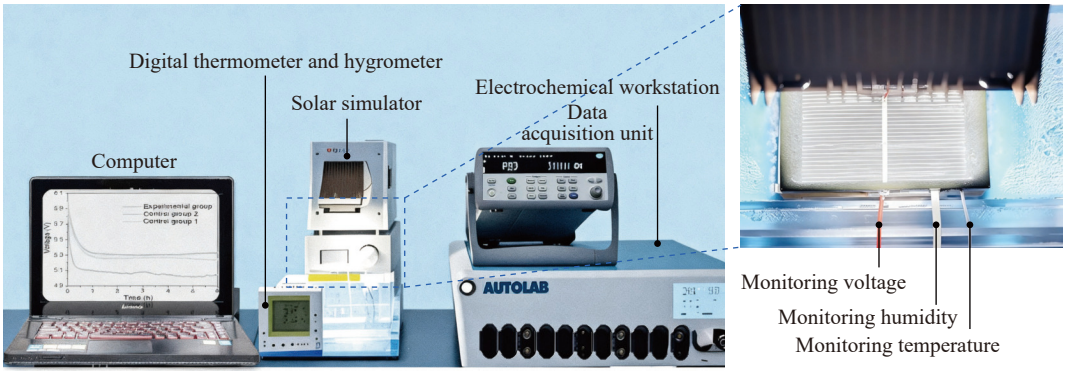

Fig. 2. Optical images showing the testing device.



Fig. 3. Illustrative diagram showing the working principle of the RTPC device.

condensation of vapor but also enables collection of the waste heat to facilitate evaporation, thereby providing a humid environment for the absorption process.

The water cycle of the RTPC system primarily involves evaporation, condensation, adsorption, and desorption. The evaporative cooling device is positioned at the top of the system. During the day, heat generated by the solar cell is dissipated through the evaporation of water within the hydrogel, forming water vapor that spreads out. The phase change of water absorbs heat from the solar cell, aiding in the cooling of the solar cell. The water vapor then diffuses downward and condenses upon contact with the walls of the water tank. The moisture in the lower layer is evaporated under the combined effects of the waste heat and the heat released from the condensation, creating an enclosed RTPC system with a high-humidity environment. This will promote the absorption of moisture by the hydrogel. As a result, a cycle of adsorption and desorption of the hydrogel is achieved, allowing for the continuous regeneration of the cooling capacity. In darkness, the solar cell enters a dormant phase, during which the adsorption capacity of the hydrogel exceeds its desorption capacity. In the high-humidity environment provided by the RTPC system, the hydrogel continues to adsorb moisture, preparing for a new cycle of solar cell cooling the following day. This approach fundamentally avoids the weakness of the hydrogel having low adsorption capacity at low humidity levels.

B. Adsorption and Water Retention

To achieve the peak cooling performance of LHAH on solar cells within the RTPC configuration, LHAHs with varying thicknesses were prepared using the *in-situ* polymerization method [41]. For convenience, samples with thicknesses of 4, 6, 8, 10, and 12 mm are designated as LHAH-4, LHAH-6, LHAH-8, LHAH-10, and LHAH-12, respectively. Post freeze-drying, the weights of these hydrogels are precisely 2.3, 3.3, 4.8, 6.6, and 7.5 g, corresponding to their respective thicknesses (Fig. 4(a)). Upon 48 h of immersion in a LiCl solution with a concentration of 0.4 $g \cdot mL^{-1}$, the weights of LHAH escalate to 15.3, 19.5, 33.1, 31.5, and 30.8 g, respectively. A discernible trend indicates that although the dry weight of the hydrogel escalates with thickness, the absorption of LiCl solution peaks at 8 mm. The LiCl loading rate, a pivotal metric measuring the amount of LiCl per unit mass, is observed to culminate in LHAH-8, with a loading rate of 5.9 $g \cdot g^{-1}$. Due to the special properties of LiCl hygroscopic salt loaded on LHAH, the increase in polar groups on the surface leads to an increase in effective polar (hydrophilic) groups. This enhancement is evidenced by the swift dispersion and absorption of a droplet into the LHAH within a mere 0.21 s (Fig. 4(b)). Experimental results demonstrate that hydrogels enriched with lithium chloride are instrumental in sustaining elevated adsorption levels across a spectrum of environmental conditions, from arid to humid. For the purpose of exploring how humidity affects the adsorption performance of LHAH, the materials were incubated in a constant temperature and humidity test chamber (HYH-150C, Huanyi) at RH levels of 60% and 90%, respectively. They undergo a continuous adsorption phase for 10 h. The ensuing adsorption rates for these hydrogels are delineated in Fig. 4(c) and Fig. 4(d). Across all thick-

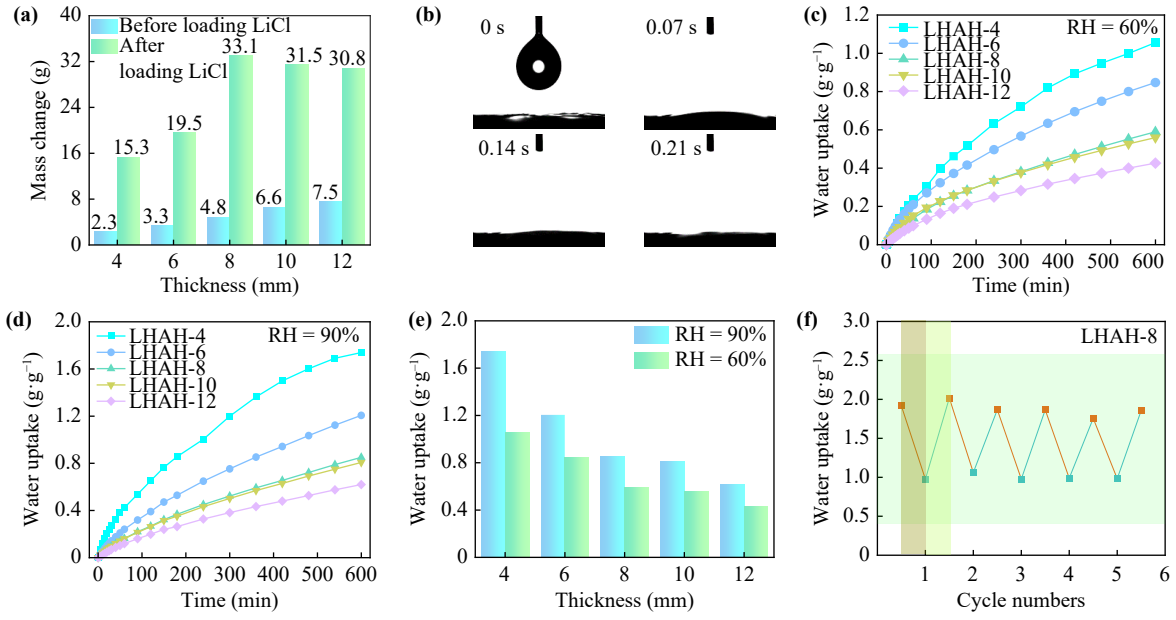

Fig. 4. The adsorption capabilities of the LHAH. (a) The mass change of LHAHs shows the loading amounts of LiCl after soaking. (b) CCD images showing the contact angle measurement of LHAH-8. The mass change rate of LHAH with varying thicknesses under (c) RH = 60% and (d) RH = 90%. The ambient temperature is 25 °C. (e) Water retention per unit mass of LHAH at RH = 60% and 90%. (f) Adsorption–desorption characteristics during the cycling process of LHAH-8.

nesses, the LHAH exhibits a more rapid adsorption rate at RH = 90% compared to RH = 30%. In addition, the adsorption rate is observed to decelerate if the thickness is increased. At RH = 90%, LHAH-8, LHAH-10, and LHAH-12 register adsorption rates of 0.9, 0.8, and 0.6 $g \cdot g^{-1}$, respectively, without surpassing their weight. This phenomenon can be attributed to the increased resistance to vapor and liquid transport within the LHAH as its thickness augments, whereas a thinner LHAH facilitates a more expeditious adsorption dynamic. [42]. These allow the RTPC to offer a more enclosed system compared to open setups, fostering a high-humidity milieu for LHAH.

Taking into account that the adsorption rate of LHAH is a function of its weight across varying humidity, it is observed that a thicker hydrogel acquires more mass at the outset. Consequently, the total water absorption capability of LHAH under different relative humidities over 10 h was scrutinized. As illustrated in Fig. 4(e), the LHAH-4 exhibits a water storage capacity of 1.1 and 1.7 $g \cdot g^{-1}$ at RH = 60% and 90%, respectively. Interestingly, as thickness increases, there is a noted decline in the water storage capacity per unit mass of the hydrogel. Nonetheless, when focusing on water absorption alone, the LHAH-6 stands out with the greatest storage capacity.

It should be highlighted that a thicker hydrogel generally possesses a higher degree of crosslinking among polymer chains, which intertwine to create a more resilient network [43]. This will enhance the mechanical strength and toughness of the LHAH. The LHAH-8, owing to its increased thickness, yields a more compact gel structure and enhanced toughness when compared to LHAH-4, rendering it well-suited for deployment across a range of complex environments. In light of this, an adsorption–desorption cycling performance test was undertaken with the LHAH-8. It was subjected to an environment of 25 °C and RH = 90% for a adsorption period of 10 h, followed by a transfer to conditions of 80 °C and RH = 10% to facilitate desorption. The dry weight, as well as its weights post-adsorption and post-desorption, was measured in a cycle that was repeated 5 times. The outcomes of the test confirm that the LHAH-8 possesses stable adsorption and desorption performance (Fig. 4(f)).

C. Water Harvesting Capacity

The designed apparatus is utilized to test the water production performance of LHAH under 1.0 sun illumination. LHAH is cut into squares the same size as the solar cells (8 cm × 8 cm) and attached to the back of the solar cells. As the solar cell operates, the generated heat is transferred downward to the LHAH. The moisture within the LHAH undergoes a desorption process due to the residual heat, forming water vapor [44]. This water vapor diffuses downward and condenses upon contact with the walls of the condensation chamber (Fig. 5(a)). The condensed water is collected by the lower water collection tank, thereby completing the water collection process. The mass of the collected water over a 2-h operation is shown in Fig. 5(b). As the thickness increases, the water collection capacity of the LHAH first increases and then decreases, with LHAH-8 collecting the most water, reaching 3.8 g. Although the adsorption rate and water storage capacity of the LHAH-4 and LHAH-6 are relatively high, when adsorbing the same mass of water, their surface areas are also larger, resulting in a lower water content per unit area. Therefore, when cutting the hydrogel into squares the same size as the solar cells, the water content of the LHAH-4 and LHAH-6 is lower. Based on this, six cyclic water collection experiments were conducted on

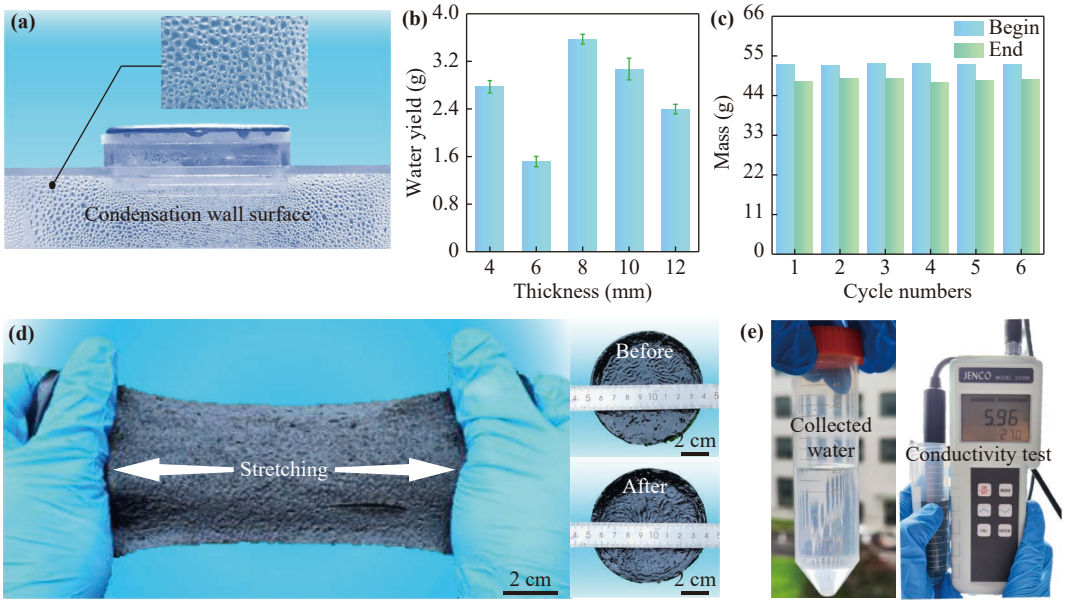

Fig. 5. Water collection experiment of the RTPC system. (a) Optical image of the water collection device. (b) Water collection amounts by hydrogels of varying thicknesses. (c) Quality changes before and after each water collection cycle for LHAH-8. (d) Tensile test image of LHAH-8 and the shape change of the sample before and after stretching. (e) The conductivity of water collected in the experiment.

LHAH-8 to verify its water collection stability. The experimental results, as shown in Fig. 5(c), indicate that the mass of the LHAH-8 before and after 6 water collection experiments is identical, and the sample structure remains intact without any damage at the end of the experiments. Combined with the excellent mechanical properties of the LHAH-8 (Fig. 5(d)), it is known that the LHAH-8 has good cyclic performance. The water quality obtained was measured, and the purity of the condensed water was detected using electrical conductivity as an indicator, finding that the collected clean water has a conductivity of 5.96 $mS \cdot cm^{-1}$ (Fig. 5(e)).

D. Humidity Regulation for RTPC System

Recognizing that the ambient humidity significantly influences the adsorption capabilities of hydrogels, and given that the hydrogel desorption is predominantly powered by the residual heat from the backboard, regulating humidity is therefore crucial for optimizing the LHAH adsorption–desorption cycle and reducing the temperature of solar cells [44]. Leveraging the thermal conductivity of LHAH and capitalizing on its propensity for adsorption in humid conditions, coupled with its high-temperature-driven evaporation, we crafted various high-humidity environments by performing different surface coverages (Fig. 6(a)–Fig. 6(c)). In the uncovered RTPC setup, the spatial volume and the lower water reservoir are warmed by solar irradiation. When fully covered, they are not heated, and with partial cover, only a section is irradiated.

The temperature and humidity of the RTPC system were adjusted by setting different volumes of water layers at 0, 100, 200, and 400 mL. When the RTPC system is fully enclosed (Fig. 6(d)), the absence of a water layer at the base, that is, at 0 mL, confines the humidity of the system to levels below 50%. Conversely, systems equipped with water layers at the base consistently maintain humidity above 70%, with the 200 mL water layer demonstrating the most rapid ascent in humidity, peaking at 83% before settling to a steady 70% after 30 min of experimentation. Notably, the system with a 400 mL water layer exhibits the most sluggish humidity increase. Within the uncovered RTPC system (Fig. 6(e)), introducing either a 100 mL or a 200 mL water layer yields analogous humidity profiles after an initial 5 min. The humidity environment created by setting a 400 mL water layer, while still lower than that of a system with a 200 mL layer, is improved compared to a fully enclosed RTPC system. This is because, in the uncovered system, the water layer also receives solar radiation. The environmental humidity in the semi-covered system showed a similar pattern to the uncovered system (Fig. 6(f)), with the 200 mL water layer at the base again leading to humidity escalation, achieving the same peak and stabilization points as previously noted.

E. Real-Time Passive Solar Cell Cooling Performance

Based on the preceding analysis, an LHAH-8 has been strategically chosen to serve as the adsorbent medium, complemented by a 200 mL water layer as the condensation component within the RTPC system. The assembly is subjected to adaptive testing under a solar intensity of 1.0 sun, with a semi-shaded canopy overhead. The experimental setup includes an LHAH-8 coupled with a 200 mL water layer within the RTPC framework, in stark contrast to the control groups 1 and 2, which lack the water layer and both the hydrogel and water layer, respectively. An infrared thermal imaging analyzer was deployed to assess and compare the average surface temperature (T_{avg}) of the solar cells across the experimental and control configurations under the specified solar conditions, as illustrated in Fig. 7(a)–Fig. 7(c). Control group 2, which is bereft of cooling mechanisms, experiences a relentless rise in surface temperature from 37.9 to 71.7 °C, peaking at 70.3 °C

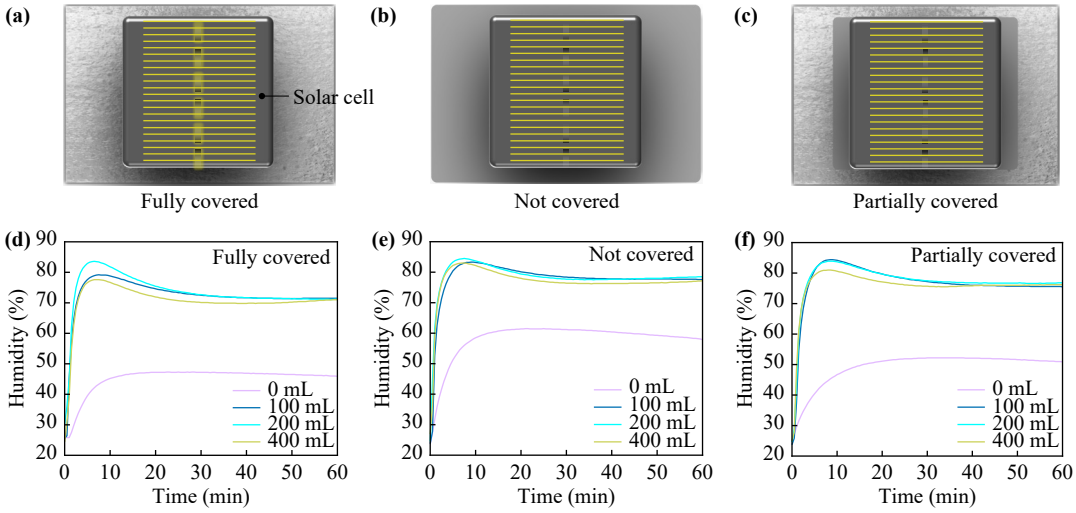

Fig. 6. System humidity regulation. Schematic diagram of solar cells with (a) tinfoil full coverage, (b) tinfoil no coverage, and (c) tinfoil partial coverage (except for solar cells, there is a total of 2 cm × 8 cm exposed). Humidity changes inside the RTPC system under different water volume adjustments for (d) tinfoil full coverage, (e) tinfoil no coverage, and (f) tinfoil partial coverage.

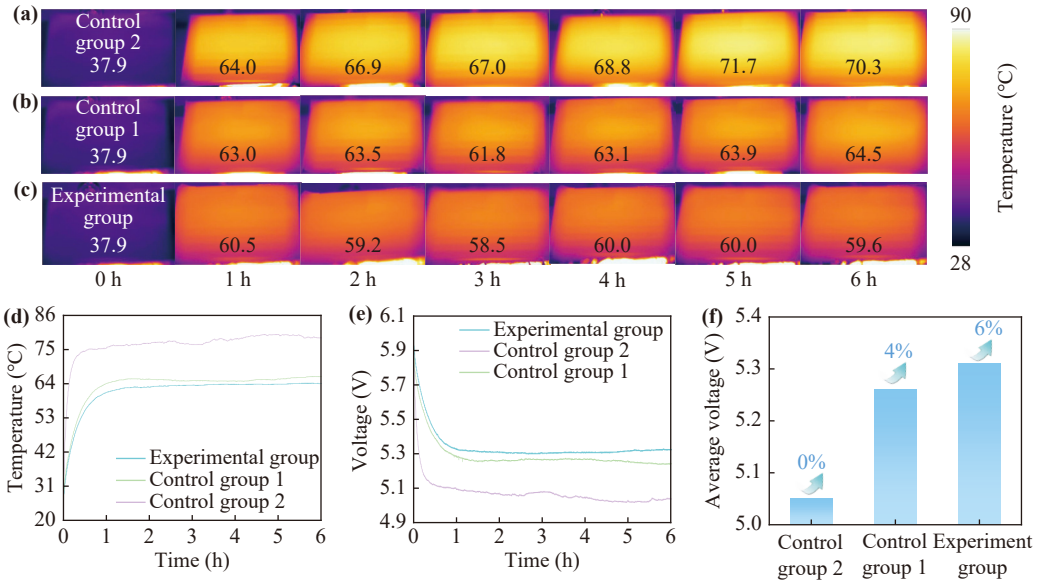

Fig. 7. The cooling and voltage boosting effects of RTPC. (a) Control group 2, (b) control group 1, and (c) experimental group surface temperature distribution. (d) Backplate temperature changes and (e) open-circuit voltage changes of the solar cells for control group 2, control group 1, and the experimental group under 1.0 sun illumination. (f) The final average voltage of the three experiments, as well as the voltage rise rates of control group 1 and experimental group relative to control group 2.

after a duration of 6 h. In contrast, control group 1, endowed with LHAH cooling, exhibits a swift ascent to 63.5 °C within the initial 2 h, thereafter settling at 61.8 °C. Nonetheless, at the 4 h mark, the temperature suddenly rose to 63.1 °C and continued to increase thereafter, reaching 64.5 °C by the end of the 6 h. Control group 1 records a 5.8 °C reduction in temperature for the solar cells compared to control group 2 after the period of 6 h. The abrupt increase at the 4 h mark is due to moisture evaporation, which compromises the cooling efficacy of the hydrogel, underscoring the inability of the group to maintain long-term cooling for the solar cells. Conversely, the average surface temperature of the solar cells in the experimental group remained consistently at 59.6 °C throughout the lengthy experimental process of 6 h, achieving a temperature reduction of 10 °C compared to control group 2, which had no configurations, until the end of the experiment. This demonstrated that the RTPC system, equipped with hygroscopic gel and condensate water, achieved long-duration adaptive cooling.

To determine the cooling effect of the three systems on the battery panel, the backplate temperatures of the solar cells are measured and obtained, with the results depicted in Fig. 7(d). Under 1.0 sun, the backplate temperature of the solar cells in control group 2 reaches relative stability within 0.5 h and then gradually ascends, culminating at 78 °C after 6 h. Control group 1 attains stability within 1 h and, under the influence of LHAH evaporative cooling, maintains this stability at 64 °C for the subsequent 3 h. However, at the 4 h mark, the temperature rise phenomenon mirrors the phenomenon observed in the surface temperature of the solar cells, with the backplate temperature reaching 66 °C by the conclusion of the 6 h period. Due to the harmonization of the solar cell temperature rise with the evaporative cooling effect of LHAH, the backplane temperature of the solar cell in the experimental group exhibited the same delayed stabilization issue as control group 1, stabilizing after about 1 h. However, under the influence of the RTPC system, it remained stable at around 63 °C, achieving a temperature reduction of 15 °C compared to control group 2.

Illuminating the scene under 1.0 sun conditions, the experimental and control groups' real-time open-circuit voltages, meticulously tested with an electrochemical workstation, are elegantly captured in Fig. 7(e). Control group 2, devoid of LHAH, undergoes a precipitous voltage decline from 6.0 to 5.1 V within the initial 30 min, thereafter gently settling to 5.0 V. In stark contrast, control group 1, endowed solely with the LHAH, observes a sharp voltage reduction from 6.0 to 5.4 V over the same interval, followed by a gradual retreat to 5.2 V. Compared to control group 2, the open-circuit voltage of control group 1 increased by 0.2 V at the end of the 6 h period. In the experimental group based on the RTPC system, the open-circuit voltage rapidly decreased from 6.0 to 5.4 V within 30 min, then gradually dropped to 5.3 V, and remained stable. Compared to control group 2, an increase of 0.3 V in open-circuit voltage was achieved, with an average open-circuit voltage increase of 6.0% (Fig. 7(f)). Notably, the open-circuit voltage of control group 2 showed a declining trend after 4 h, which is consistent with the surface temperature changes of the solar cell captured by the infrared camera after 4 h. This indicates that using LHAH-8 hydrogel as the cooling material and a 200 mL water layer as the condensation layer for the RTPC system, the top half-covered RTPC system compensates for the shortcomings of using only hydrogel as a cooling material in an open space for continuous operation [45]. It not only supplies moisture but also maintains the cool-

ing effect of solar cells, enhancing the average open-circuit voltage, outperforming most previously reported water-electricity generation configurations [46], [47], [48], [49], [50], [51], [52], [53], [54]. Furthermore, it is emotionally defensible that the price of RTPC devices is an important decisive factor for consumers to decide to blend in with the solar-to-water market. The preparation method described in Section II.B is a low-cost and straightforward approach to obtaining high-quality hydrogels. Due to the accessibility and low price of the raw material we used (nano-carbon and acrylic plates), the cost of RTPC is approximately 2.1 $, with the cost primarily contributed by nano-carbon powder. Notably, thanks to the rapid development of nanotechnology, the production cost of nanomaterials decreases annually. It should also be noted that if large-scale production of RTPC is realized, it will be available at a lower price.

IV. Conclusion

This study addresses the critical challenge of temperature elevation in solar cells operating under arid conditions, which degrades their operational efficiency, by proposing an eco-friendly passive humidification strategy. This approach harnesses the waste heat emitted by solar cells to propel the generation of pure water via LHAH, establishing a proficient and relentless solar cell cooling mechanism. The findings illustrate that the LiCl loading rate for LHAH-8 soars to 5.9 $g \cdot g^{-1}$, accumulating a water collection yield of 3.8 g with an electrical conductivity of 5.96 $mS \cdot cm^{-1}$. Moreover, the system of resilience is underscored by its stable performance across 5 consecutive cyclic water collection trials, attesting to its commendable reusability. The RTPC system, under 1.0 sun illumination, reduced the average surface temperature and backplate temperature of the solar cells by approximately 10 and 15 °C, respectively, and increased the open-circuit voltage and average open-circuit voltage by 0.3 V and 6.0%, respectively. The RTPC system is suitable for arid/semi-arid photovoltaic power plants and distributed and portable PV devices, and meets the needs of water shortage/no external energy scenarios with low water consumption and self-sustaining characteristics. However, the industrialization needs to solve the core challenges, such as the potential corrosion of LiCl on PV modules, the durability of hydrogel outdoor machinery, and the cost control of large-scale preparation.

Declaration of Competing Interest

The authors declare that they have no known competing financial interests or personal relationships that could have appeared to influence the work reported in this paper.

Funding

This work was supported by the National Natural Science Foundation of China (No. 52276148).

AI Usage Statement

During the preparation of this manuscript, the authors used AI-assisted tools for language polishing only. The authors have reviewed and edited the content and take full responsibility for the final version of the manuscript.

References

[1] S. Kim, J. H. Park, J. W. Lee, Y. Kim, and Y. T. Kang, "Self-recovering passive cooling utilizing endothermic reaction of NH_4NO_3/H_2O driven by water sorption for photovoltaic cell," *Nat. Commun.*, vol. 14, no. 1, pp. 2374, Apr. 2023.

[2] T. Kirchartz, G. H. Yan, Y. Yuan, B. K. Patel, D. Cahen, and P. K. Nayak, "The state of the art in photovoltaic materials and device research," *Nat. Rev. Mater.*, vol. 10, no. 5, pp. 335–354, Mar. 2025.

[3] N. Yang, Y. Cui, W. Fu, X. L. Ma, T. Zhang, W. X. Wang, Y. Xiao, Z. H. Chen, Q. Kang, G. Z. Zuo, and J. H. Hou, "Low-cost narrow-bandgap organic semiconductor for efficient photovoltaic and photodetection applications," *ACS Energy Lett.*, vol. 10, no. 5, pp. 2468–2476, Apr. 2025.

[4] Z. W. Zhou, Y. T. Zhang, W. J. Liu, C. X. Gui, L. Huang, H. W. Huang, K. Fan, Y. N. Huang, Y. H. Gong, A. F. Chen, P. Liu, and H. F. Jiang, "Photovoltaic cooling and atmospheric water harvesting using a hygroscopic hydrogel," *Desalination*, vol. 583, pp. 117685, Aug. 2024.

[5] S. Y. Chan, K. Chen, K. F. Hu, L. F. Shi, Y. Pei, B. Zhao, and G. Pei, "Comparative analysis of switchable natural cooling methods for efficient thermal management in photovoltaic/thermal collectors," *Appl. Energy*, vol. 385, pp. 125499, May 2025.

[6] E. Mariam, B. Ramasubramanian, V. S. Reddy, G. K. Dalapati, S. Ghosh, T. Sherin PA, S. Chakrabortty, M. R. Motapothula, A. Kumar, S. Ramakrishna, and S. Krishnamurthy, "Emerging trends in cooling technologies for photovoltaic systems," *Renew. Sustain. Energy Rev.*, vol. 192, pp. 114203, Mar. 2024.

[7] S. Lv, J. W. Ren, Q. L. Zhang, B. L. Zhang, Y. Lai, J. H. Yang, Z. H. Chang, and Z. P. Zhan, "Design, fabrication and performance analysis of a cost-effective photovoltaic interface seawater desalination hybrid system for co-production of electricity and potable water," *Appl. Energy*, vol. 336, pp. 120811, Apr. 2023.

[8] N. Xu, P. C. Zhu, Y. Sheng, L. Zhou, X. Q. Li, H. R. Tan, S. N. Zhu, and J. Zhu, "Synergistic tandem solar electricity-water generators," *Joule*, vol. 4, no. 2, pp. 347–358, Feb. 2020.

[9] D. Lopez-Pascual, I. Valiente-Blanco, M. Fernandez-Munoz, and E. Díez-Jiménez, "Theoretical modelling and optimization of a geothermal cooling system for solar photovoltaics," *Renew. Energy*, vol. 206, pp. 357–366, Apr. 2023.

[10] A. M. Bukar, A. Almerbati, S. Z. Shuja, and S. M. Zubair, "Enhancing solar PV panel performance through active and passive cooling techniques: a comprehensive review," *Renew. Sustain. Energy Rev.*, vol. 216, pp. 115611, Jul. 2025.

[11] M. Firoozzadeh, A. H. Shiravi, and S. Hodaei, "An experimental approach on employing air flow through a porous medium as coolant of photovoltaic module: Thermodynamics assessment," *Ther. Sci. Eng. Prog.*, vol. 40, pp. 101799, May 2023.

[12] R. Gad, H. Mahmoud, and H. Hassan, "Performance evaluation of direct and indirect thermal regulation of low concentrated (via compound parabolic collector) solar panel using phase change material-flat heat pipe cooling system," *Energy*, vol. 274, pp. 127323, Jul. 2023.

[13] K. P. Shan, Q. Z. Luo, P. F. Yun, L. Huang, K. M. Huang, B. Cao, B. Tang, and H. F. Jiang, "All-day working photovoltaic cooling system for simultaneous generation of water and electricity by latent heat recycling," *Chem. Eng. J.*, vol. 457, pp. 141283, Feb. 2023.

[14] W. B. Wang, S. Aleid, Y. F. Shi, C. L. Zhang, R. Y. Li, M. C. Wu, S. F. Zhuo, and P. Wang, "Integrated solar-driven PV cooling and seawater desalination with zero liquid discharge," *Joule*, vol. 5, no. 7, pp. 1873–1887, Jul. 2021.

[15] Y. M. Liu, Z. B. Liu, Z. P. Wang, W. M. Sun, and F. Z. Kong, "Photovoltaic passive cooling via water vapor sorption-evaporation by hydrogel," *Appl. Ther. Eng.*, vol. 240, pp. 122185, Mar. 2024.

[16] D. H. El-Nagar, M. Emam, A. A. El-Betar, and S. A. Nada, "Combining active and passive cooling techniques for maximizing power generation and thermal utilization of photovoltaic panels," *Renew. Energy*, vol. 250, pp. 123310, Sep. 2025.

[17] S. Nižetić, D. Čoko, A. Yadav, and F. Grubišić-Čabo, "Water spray cooling technique applied on a photovoltaic panel: the performance response," *Energy Convers. Manage.*, vol. 108, pp. 287–296, Jan. 2016.

[18] J. Li, Z. Y. Hu, Y. J. Xue, J. M. Li, and H. C. Zhang, "Actively cooling photovoltaic modules and simultaneously yielding freshwater via humidifier-dehumidifiers: performance predictions and regulatory strategies, " *Appl. Ther. Eng.* , vol. 268, pp. 125909, 2025.

[19] X. T. Zhao and J. F. Pan, "Keeping photovoltaics cool," *Joule*, vol. 9, no. 2, pp. 101845, Feb. 2025.

[20] S. S. Koohestani, S. Nižetić, and M. Santamouris, "Comparative review and evaluation of state-of-the-art photovoltaic cooling technologies," *J. Cleaner Prod.*, vol. 406, pp. 136953, Jun. 2023.

[21] I. Čorić, S. Nižetić, and M. Jurčević, "Progress in passive cooling strategies for silicon photovoltaic panels with incorporated phase change materials," *Energy*, vol. 327, pp. 136370, Jul. 2025.

[22] Z. Y. Mao, Y. Yao, Y. H. He, Z. Yu, Y. C. Han, J. D. Shen, X. X. Tang, F. C. Lyu, M. L. Miao, Y. X. Xu, Z. Song, X. G. Duan, Y. H. Su, H. X. Yang, Q. L. Wang, and J. Lu, "Passively ultra cooling patch enabling high-efficiency power-water cogeneration," *Adv. Mater.*, vol. 38, no. 2, pp. e05002, Jan. 2026.

[23] S. V. Hudișteanu, F. E. Țurcanu, N. C. Cherecheș, C. G. Popovici, M. Verdeș, and I. Huditeanu, "Enhancement of PV panel power production by passive cooling using heat sinks with perforated fins," *Appl. Sci.*, vol. 11, no. 23, pp. 11323, Nov. 2021.

[24] K. Wang, G. L. Luo, X. W. Guo, S. R. Li, Z. J. Liu, and C. Yang, "Radiative cooling of commercial silicon solar cells using a pyramid-textured PDMS film," *Sol. Energy*, vol. 225, pp. 245–251, Sep. 2021.

[25] B. Utomo, J. Darkwa, D. F. Du, and M. Worall, "Solar photovoltaic cooling and power enhancement systems: a review," *Renew. Sustain. Energy Rev.*, vol. 216, pp. 115644, Jul. 2025.

[26] X. B. Xu, J. J. Shen, W. J. Dong, X. L. Wang, H. Y. Zhang, and F. Zhou, "Development and performance analysis of a multifunctional composite phase change cooling plate for improving battery thermal management," *Appl. Ther. Eng.*, vol. 266, pp. 125762, May 2025.

[27] W. C. Fu, X. Yan, Y. Gurumukhi, V. S. Garimella, W. P. King, and N. Miljkovic, "High power and energy density dynamic phase change materials using pressure-enhanced close contact melting," *Nat. Energy*, vol. 7, no. 3, pp. 270–280, Mar. 2022.

[28] J. Luo, D. Q. Zou, Y. S. Wang, S. Wang, and L. Huang, "Battery thermal management systems (BTMs) based on phase change material (PCM): A comprehensive review," *Chem. Eng. J.*, vol. 430, pp. 132741, Feb. 2022.

[29] Z. G. Sui, Y. R. Sui, Z. X. Ding, H. S. Lin, F. X. Li, R. G. Yang, and W. Wu, "Membrane-encapsulated, moisture-desorptive passive cooling for high-performance, ultra-low-cost, and long-duration electronics thermal management," *Device*, vol. 1, no. 6, pp. 100121, Dec. 2023.

[30] M. Hasanuzzaman, A. B. M. A. Malek, M. M. Islam, A. K. Pandey, and N. Abd Rahim, "Global advancement of cooling technologies for PV systems: a review," *Sol. Energy*, vol. 137, pp. 25−45, 2016.

[31] S. Li, K. Shao, X. C. Wu, S. X. Wang, J. J. Li, C. Guo, L. M. Yu, P. Murto, and X. F. Xu, "Self-contained moisture management and evaporative cooling through 1D to 3D hygroscopic all-polymer composites," *Adv. Funct. Mater.*, vol. 34, no. 9, pp. 2310020, Feb. 2024.

[32] J. L. Li, X. Y. Wang, D. Liang, N. Xu, B. Zhu, W. Li, P. C. Yao, Y. Jiang, X. Z. Min, Z. Z. Huang, S. N. Zhu, S. H. Fan, and J. Zhu, "A tandem radiative/evaporative cooler for weather-insensitive and high-performance daytime passive cooling," *Sci. Adv.*, vol. 8, no. 32, pp. eabq0411, Aug. 2022.

[33] C. X. Wang, L. J. Hua, H. Z. Yan, B. J. Li, Y. D. Tu, and R. Z. Wang, "A thermal management strategy for electronic devices based on moisture sorption-desorption processes," *Joule*, vol. 4, no. 2, pp. 435–447, Feb. 2020.

[34] Y. T. Ji, Y. L. Sun, M. Javed, Y. H. Xiao, X. Y. Li, K. L. Jin, Z. S. Cai, and B. Xu, "Skin inspired thermoresponsive polymer for constructing self-cooling system," *Energy Convers. Manage.*, vol. 254, pp. 115251, Feb. 2022.

[35] Y. H. Guo, J. Bae, Z. W. Fang, P. P. Li, F. Zhao, and G. H. Yu, "Hydrogels and hydrogel-derived materials for energy and water sustainability," *Chem. Rev.*, vol. 120, no. 15, pp. 7642–7707, Jul. 2020.

[36] W. W. Wang, J. W. Chen, C. Y. Zhang, H. F. Yang, X. W. Ji, H. L. Zhang, F. Y. Zhao, and Y. Cai, "Green thermal management of photovoltaic panels by the absorbent hydrogel evaporative (AHE) cooling jointly with 3D porous copper foam (CF) structure," *Energy*, vol. 293, pp. 130467, Apr. 2024.

[37] S. Boon-In, M. Theerasilp, and D. Crespy, "Temperature-responsive double-network cooling hydrogels," *ACS Appl. Polym. Mater.*, vol. 5, no. 4, pp. 2562–2574, Mar. 2023.

[38] S. R. Pu, J. Fu, Y. T. Liao, L. R. Ge, Y. H. Zhou, S. L. Zhang, S. L. Zhao, X. W. Liu, X. J. Hu, K. Liu, and J. Chen, "Promoting energy efficiency via a self-adaptive evaporative cooling hydrogel," *Adv. Mater.*, vol. 32, no. 17, pp. 1907307, Apr. 2020.

[39] L. Yu, Y. M. Huang, Y. W. Zhao, Z. H. Rao, W. H. Li, Z. Chen, and M. J. Chen, "Self-sustained and insulated radiative/evaporative cooler for daytime subambient passive cooling," *ACS Appl. Mater. Interfaces*, vol. 16, no. 5, pp. 6513–6522, Jan. 2024.

[40] T. Zhu, C. Jiang, M. L. Wang, C. Z. Zhu, N. Zhao, and J. Xu, "Skin-inspired double-hydrophobic-coating encapsulated hydrogels with enhanced water retention capacity," *Adv. Funct. Mater.*, vol. 31, no. 27, pp. 2102433, Jul. 2021.

[41] R. Y. Li, Y. Shi, M. Alsaedi, M. C. Wu, L. Shi, and P. Wang, "Hybrid hydrogel with high water vapor harvesting capacity for deployable solar-driven atmospheric water generator," *Environ. Sci. Technol.*, vol. 52, no. 19, pp. 11367–11377, Sep. 2018.

[42] C. D. Díaz-Marín, L. N. Zhang, Z. M. Lu, M. Alshrah, J. C. Grossman, and E. N. Wang, "Kinetics of sorption in hygroscopic hydrogels," *Nano Lett.*, vol. 22, no. 3, pp. 1100–1107, Jan. 2022.

[43] Z. Y. Zhu, H. J. Yu, L. Wang, J. W. He, Y. H. Zhang, Y. L. Wang, Y. Zhang, C. G. Ouyang, and Y. G. Lu, "Advances in hygroscopic hydrogels for atmospheric water harvesting applications," *J. Environ. Chem. Eng.*, vol. 13, no. 5, pp. 119047, Oct. 2025.

[44] B. L. Bai, S. Du, and M. J. Li, "Photovoltaic efficiency improved by self-adaptive water uptake hydrogel evaporative cooling," *Appl. Energy*, vol. 383, pp. 125367, Apr. 2025.

[45] L. Xu, D. W. Sun, Y. Tian, L. B. Sun, and Z. W. Zhu, "Self-rehydrating and highly entangled hydrogel for sustainable daytime passive cooling," *Chem. Eng. J.*, vol. 479, pp. 147795, Jan. 2024.

[46] Y. Ding, X. R. Huang, Y. Hu, X. Y. Zhao, G. C. Lu, C. Zhou, S. L. Liu, X. Lu, and J. P. Qu, "Boosting photovoltaic efficiency via efficient passive cooling from all-natural hydrogels with robust interfacial adhesion," *J. Energy Chem.*, vol. 114, pp. 206–216, Mar. 2026.

[47] Y. Hu, T. Guo, X. Y. Qu, T. F. Xu, B. T. Huang, and T. Y. Xie, "Enhanced passive radiative cooling of cementitious composites for efficient photovoltaic thermal management," *Energy Convers. Manage.*, vol. 344, pp. 120268, Nov. 2025.

[48] X. T. Xie, Y. Liu, Y. P. Zhang, H. X. Xie, J. Y. Ye, H. J. Li, and W. F. Chen, "Photovoltaic efficiency enhancement via responsive forced convection driven by radiative-cooling-intensified thermoelectricity," *Chem. Eng. J.*, vol. 521, pp. 166606, Oct. 2025.

[49] J. X. Li, C. J. Xu, L. F. Chen, X. H. Zhang, M. F. Zhu, and Y. H. Cheng, "Tandem atmospheric water harvesting and passive cooling enabled by hygroscopic biopolymer-based aerogels," *Adv. Funct. Mater.*, vol. 35, no. 31, pp. 2423063, Aug. 2025.

[50] H. Y. Fang, S. C. Dang, P. Kumar, J. K. Wang, L. J. Xu, Y. K. Zhu, A. Almogbel, A. Albadri, S. De Wolf, and Q. Q. Gan, "Streamlined fabrication of an inexpensive hygroscopic composite for low maintenance evaporative cooling of solar panels," *Mater. Sci. Eng. R: Rep.*, vol. 165, pp. 101016, Jul. 2025.

[51] W. W. Zou, M. X. Ji, C. Han, E. Z. Tian, and J. H. Mo, "Enhancing the internal thermal conductivity of hydrogel for efficient passive heat dissipation: experimental study of a surface simulating a cooled photovoltaic panel," *Energy Convers. Manage.*, vol. 306, pp. 118328, Apr. 2024.

[52] J. Shang, J. H. Zhang, Y. H. Zhang, X. Y. Zhang, and Q. An, "Highly potent transparent passive cooling coating via microphase-separated hydrogel combining radiative and evaporative cooling," *Nano Lett.*, vol. 24, no. 1, pp. 7055–7062, May 2024.

[53] M. Han, K. Jiao, L. Lu, Z. P. Jin, T. Ma, and Q. W. Wang, "PEG-based solid-solid phase change materials for passive cooling of solar photovoltaic panels," *Appl. Energy*, vol. 394, pp. 126190, Sep. 2025.

[54] Z. P. Li, T. Ma, F. Ji, H. Shan, Y. J. Dai, and R. Z. Wang, "A hygroscopic composite backplate enabling passive cooling of photovoltaic panels," *ACS Energy Lett.*, vol. 8, no. 4, pp. 1921–1928, Mar. 2023.



Yuan Chang is currently a Ph.D. candidate at Northeast Electric Power University, Jilin, China. His research interests include high-efficiency solar energy utilization and low-carbon power technologies.

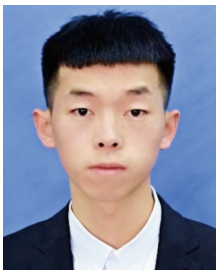

Wei Yan obtained his M.S. degree in Energy and Power Engineering from Northeast Electric Power University, Jilin, China in 2024 and is currently employed by State Grid Corporation of China.



Haoran Li earned his Ph.D. degree in School of Energy Science and Engineering from Harbin Institute of Technology, China. He is currently an Associate Professor at the School of Energy and Power Engineering, Northeast Electric Power University, China. His research interests include photovoltaic hydrogen production and high flux heat dissipation.



Wenpeng Hong is Dean of the School of Energy and Power Engineering, Northeast Electric Power University, China. His main research interests include low-carbon energy devices and equipment.



Yurong He is a Professor and doctoral supervisor at the School of Energy Science and Engineering, Harbin Institute of Technology, China, and a member of the Institution of Chemical Engineers (IChemE), U.K. Her research focuses on multiphase flow and thermophysics issues in energy utilization, covering mesoscience of particle-fluid systems, and thermal management of ultra-high heat flux devices.